Heliyon 8 (2022) e11125

Contents lists available at ScienceDirect

Heliyon

journal homepage: www.cell.com/heliyon

Research article

# Isolation, characterization and anti-UVB irradiation activity of an extracellular polysaccharide produced by *Lacticaseibacillus rhamnosus* VHPriobi O17

Shudong Peng [a,b], Chaoqun Guo [c], Songjie Wu [c], Zhi Duan [c,*]

[a] School of Food Science and Engineering, South China University of Technology, Guangzhou, China
[b] Guangdong Youmei Institute of Intelligent Bio-Manufacturing, Foshan, 528225, China
[c] Qingdao Vland Biotech Inc. Nutrition and Health Technology Center, Qingdao, China

ARTICLE INFO

*Keywords:*
Exopolysaccharides
*Lacticaseibacillus rhamnosus*
HaCaT cells
Anti-UVB

ABSTRACT

The purpose of this study was to isolate exopolysaccharides (EPS) from lactic acid bacteria (LAB) and evaluate EPS anti-UVB viability. *Lacticaseibacillus rhamnosus* VHPriobi O17 with high EPS production was screened from 34 strains of LAB. The EPS (OP-2) produced by *L. rhamnosus* VHPriobi O17 was purified by alcohol precipitation and DEAE-μSphere anion exchange chromatography. By ion chromatography, FT-IR spectrum and gel column chromatography, EPS (OP-2) was a novel Man-like polysaccharide with the weight-averaged molecular of 84.2 kDa. The EPS (OP-2) can effectively alleviate HaCaT cells apoptosis and overproduction of reactive oxygen species (ROS) induced by UVB. The results also showed that it inhibited the release of pro-inflammatory cytokines (IL-1α, IL-6 and IL-8); and suppressed the phosphorylation cascade of JNK and p38 MAPK to reduce the expression level of active-caspase3, ultimately prevented cell apoptosis. Thus, the EPS produced by *L. rhamnosus* VHPriobi O17 have the potential to be used for human anti-UVB irradiation.

## 1. Introduction

Solar ultraviolet rays irradiated to human skin contain 90–99% UVA and 1–10% UVB, but the damage of UVB to the skin is 1000 times higher than that of UVA at the same dose [1]. There are direct and indirect ways of skin damage induced by UVB. UVB directly acts on the keratinocytes of the human epidermis and is absorbed by DNA, protein, and other molecules; which will result in cell death, mutation, and even cancer [2]. UVB irradiation can also lead to the generation of ROS, which indirectly damage skin cells. ROS activated signaling pathways, including mitogen-activated protein kinases (MAPK) and nuclear factor-κB (NF-κB), to promote apoptosis of skin cells. This process will also promote the secretion of IL-1, IL-6 and other inflammatory factors, which will stimulate the cells to produce NADPH oxidase enzymes and further lead to the production of more ROS [3].

At present, the anti-UVB activity of natural products from plants, animals and microorganisms has aroused people's interest and has been partially applied in the field of cosmetics. Studies have found that the natural flavonoid silibinin protected cells from UVB damage by up-regulating the estrogen receptors (ER) alpha and ER beta pathways [4]; trehalose resists UVB-induced skin aging by inhibiting the expression of matrix metalloproteinases (MMPs) [5]; exopolysaccharide from *Pantoea agglomerans* can protect HaCaT cells from UVB damage [6]. A recent report found that a plant material fermented with lactic acid bacteria (LAB) exhibited anti-photoaging effects [7].

Some strains of LAB are probiotics, which are live microorganisms that confer the host health benefits when ingested in sufficient amounts [8]. And certain LAB have been used in functional food and pharmaceutical fields because of their beneficial effects such as regulating immunity and balancing intestinal health. Previous studies have shown that the probiotic effect of LAB is related to its metabolites such as organic acids, antimicrobial peptides and EPS [9]. The EPS produced by LAB are a polysaccharide composed of monosaccharides, which are bound to the cell surface of bacteria in the form of capsules or secreted into the extracellular environment in the form of mucus. LAB producing EPS have been widely reported, such as *Lacticaseibacillus rhamnosus*, *Lactobacillus helveticus*, *Lactobacillus acidophilus*, *Lactiplantibacillus plantarum*, *etc* [10]. Noteworthy, Ispirli & Dertli found that the yield of EPS from *L. mesenteroides* AP40 was 5.37 g/L, while that from *L. kunkeei* AP-30 was 0.15 g/L [11]. Therefore, screening LAB with high-yield of EPS is very

* Corresponding author.
*E-mail address:* duanzhi@vlandgroup.com (Z. Duan).

https://doi.org/10.1016/j.heliyon.2022.e11125
Received 19 February 2022; Received in revised form 27 May 2022; Accepted 12 October 2022

important for industrial applications. There are many reports about the health effects of EPS produced by LAB. Di et al. reported that four strains of *L. casei* produced EPS that inhibited the growth of HT-29 cells [12]. Dinic et al. found that EPS secreted by *L. paraplantarum* BGCG11 reduced inflammation in Wistar rats [13]. Other study found that EPS from *L. acidophilus*, *L. mesenteroides* and *L. lactis* had antioxidant activity [14]. However, there are few studies on the anti-UVB irradiation and related mechanisms of EPS produced by LAB.

Accordingly, this study aimed to screen out a LAB with high-yield EPS and identify it. The EPS was purified from the supernatant of the strain and its structure was analyzed. In addition, human keratinocytes (HaCaT cells) were used to construct the UVB-induced skin injury model to study the protective effect of EPS and analyze the potential mechanism.

## 2. Materials and methods

### 2.1. Materials

The de Man Rogosa Sharpe (MRS) medium was supplied by Beijing Land Bridge Technology Co., Ltd. (Guangdong, China). DEAE-μSphere was purchased from the PAESINO (Wuxi, China). The Human keratinocytes (HaCaT cells) were obtained from Cobioer Biosciences Co., Ltd. (Ningbo, China). RIPA cell lysate, fat-free milk powder, trypsin, 3-(4,5-dimethylthiazol-2-11)-2,5-diphenyl tetrazolium bromide (MTT), polyvinylidene difluorid (PVDF) and electrochemiluminescence (ECL) solution were obtained from Solarbio Science & Technology Co. Ltd. (Beijing, China). Roswell Park Memorial Institute (RPMI) and Phosphate Buffered Saline (PBS) were purchased from HyClone (South Logan, UT, USA). Enzyme-linked immunosorbent assay (ELISA) kits for human interleukin-1α (IL-1α), interleukin-1β (IL-1β), interleukin-6 (IL-6), and interleukin-8 (IL-8) were obtained from the R&D Systems (Minneapolis, MN, USA). The primary antibody: anti-phospho-JNK, anti-phospho-p38 MAPK, anti-active-caspase3, anti-GAPDH were supplied by Abcam (UK).

### 2.2. Screening and identification of LAB producing EPS

Saliva from the mouths of 6 adults was collected. LAB were isolated by saliva gradient dilution ($10^{-1}$, $10^{-2}$, $10^{-3}$, $10^{-4}$ and $10^{-5}$) and spread on MRS plates. Isolated LAB were observed by plate whether the "ropy" phenotype. Strains with "ropy" phenomenon further detected the production of EPS. After the strain was cultured in MRS broth for 48 h, the cell-free supernatant (CFS) was obtained by centrifugation at 4000 × g for 10 min at 4 °C. Subsequently, The CFS was dialyzed against distilled water through the dialysis membrane (31 mm, 3.1 mL/cm, yuan ye Bio-Technology, China) with a retained molecular weight of 1 kDa, and distilled water was changed every 12 h. After the CFS was dialyzed, the EPS concentration was detected by the phenol-sulfuric acid method [15], and reaction results of glucose solution were used as standard curves. LAB with the highest yield of EPS was selected for further experiments.

The identification of LAB was based on the characteristics of colony morphology, protein expression and genetics. The strain was cultured on the MRS plate at 37 °C for 48 h, and then the colony morphology and Gram staining were observed [16]. Picked out the strains and spread them on the target plate, and prepared the samples according to the method of mass spectrometry sample pretreatment kit (Autobio, Zhengzhou, China). After that, the target plate was placed in MALDI TOF MS (Autof ms 1000, Autobio, China) to complete the protein profile analysis, and the data analysis was performed by Autof Acquirer V2.0.59 (Autobio, China). The genetic characteristics of the strain were analyzed as previously described [17]. Briefly, the 16S rRNA gene of the strain was extracted and amplified by the polymerase chain reaction (PCR), and then sequenced at Beijing Genomics Institute (Shenzhen, China). The phylogenetic tree was constructed using neighbor-joining in MAGE 5.0.

### 2.3. Dynamics of growth and EPS production

The 200 μL of MRS broth inoculated with LAB was added to a microplate and sealed with 50 μL of sterile glycerin. The microplate was placed in a microplate reader (Multiskan FC, Thermos Scientific, USA) and incubated at 37 °C for 56 h, and the $OD_{600}$ value was measured every 8 h. The EPS-producing LAB were inoculated into 100 mL of MRS broth, cultured at 37 °C for 56 h, and 5 mL of bacterial solution was taken every 8 h and centrifuged at 6000 × g for 10 min to obtain the CFS containing EPS. The EPS content of the CFS was assayed according to the method in section 2.2.

### 2.4. Isolation of EPS from LAB

#### 2.4.1. Isolation of EPS

The extraction of EPS of LAB according to the previously described with some modifications [18, 19]. Briefly, strain O17 was inoculated in 1 L MRS broth and aerobic fermentation was carried out at 37 °C for 40 h. The fermentation broth was heated at 100 °C for 20 min, then bacteria and denatured proteins were removed by centrifugation at 6000 × g for 10 min. Obtained the CFS was concentrated 5 times by a rotary evaporator (RE-52AA, Yarong Yiqi, China), EPS was precipitated by adding the double volume of cold absolute ethanol and staying overnight at 4 °C. After that, centrifugation at 12000 × g for 15 min was performed to gain crude EPS, and alcohol precipitation again. Trichloroacetic acid (4%, w/v) was added to the crude EPS solution, kept at 4 °C for 2 h, and protein was removed by centrifugation at 8000 × g for 15 min. After removing the protein, the solution of pH was adjusted to 4 with 6 mol/L NaOH to avoid degradation of EPS in a low pH environment, dialyzed at last.

#### 2.4.2. Anion exchange chromatography

The obtained EPS solution was carried in a chromatography column (1.2 × 11.4 cm) filled with DEAE-μSphere. The column was eluted successively by 0, 0.05, 0.1, 0.2, 0.4 and 0.6 mol/L sodium chloride at the speed of 1 mL/min, then collected the eluent at 5 mL per tube. Phenol-sulfuric acid procedure was used to detect the absorbance of each tube at 490 nm, the tubes containing EPS were consolidated based on the peak. Subsequently, dialyzed EPS was freeze-dried for further experiments.

### 2.5. Characterization of EPS

#### 2.5.1. Monosaccharide composition

Approximately 5 mg of purified EPS was treated with 1 mL of 2 M trifluoroacetic acid at 105 °C for 6 h in a sealed tube and dried the sample with nitrogen. Methanol was added to wash, then blow-dried, and the washing was repeated 3 times. The leavings were re-dissolved in deionized water and analyzed by ion chromatography (ICS5000, Thermo Fisher Scientific, USA) equipped with Carbopac PA-10 anion exchange column (4.6 × 250 mm, Dionex, USA). Chromatographic data were analyzed with the software Chromeleon 7.2.

#### 2.5.2. Molecular weight of EPS

Purified EPS solution (5 mg/mL) was transferred to inject vial after passing 0.22 μm filter membrane. A 20 μL of the sample was sucked into a BRT105-104-102 tandem gel column (8 × 300 mm, BoRui Saccharide, China) and refractive index detector (RI-10A, Shimadzu, Japan) for analysis. According to the curve of standard dextran (molecular weight is 1152, 5000, 11600, 23800, 48600, 80900, 148000, 273000, 409800, 667800 Da), the calculation formula was obtained and the weight-averaged molecular ($M_w$) of the sample was calculated.

#### 2.5.3. FT-IR analysis

The purified EPS was dried and mixed with 200 mg KBr powder, then rubbed and tabletted. The Fourier transform infrared (FT-IR) spectrometry (Nicolet 6700, Thermo Fisher Scientific, USA) was used for infrared

scanning of the EPS in the wavelength range of 4000–400 $cm^{-1}$, and recorded infrared spectrum.

### 2.6. The effect of EPS on HaCaT cells

#### 2.6.1. Cell culture

HaCaT cells were grown in RPMI medium with 10% (v/v) Fetal bovine serum and 1% (v/v) penicillin-streptomycin (Solarbio, China). Cells were cultured in a carbon dioxide incubator (RYX-150, Taisote Medical Equipment, China) at 37 °C with 5% (v/v) $CO_2$, and the medium was changed every 3 days.

#### 2.6.2. Treatment of cells with purified EPS

HaCaT cells were seeded on a 24-well plate ($2 \times 10^5$ cells per well) and incubated with a 500 μL medium for 24 h. After 24 h of culture, the medium was replaced by an RPMI medium containing 0, 1, 2, 4, 8, 16 mg/mL purified EPS and incubated for 2 h. Subsequently, each well was cultured in 500 μL of fresh RPMI medium for 24 h. The percentage of viable cells was detected by MTT assay and expressed as 100% negative control cells [20].

#### 2.6.3. UVB irradiation

HaCaT cells cultured in a 24-well plate for 24 h were treated with medium containing 0, 1, 2, 4, 8, and 16 mg/mL EPS for 2 h, respectively. After that, the medium was aspirated, adding 150 μL PBS into the well, and irradiated the cells with a UVB lamp (peak 306 nm, Nanjing Huaqiang, China). The irradiance of the UVB lamp was 250 μw/$cm^2$, radiation dose was 7.5, 15 and 30 mJ/$cm^2$. After that, cells were cultured in the medium for 24 h, and viable cells were detected by the MTT method. The inverted microscope (YJ051-M, Haosail, China) was used to observe the cell morphology. Not treated by UVB and EPS was used as a control.

#### 2.6.4. Determination of intracellular ROS and pro-inflammatory cytokines assay

HaCaT cells were treated with medium containing 0, 1, 2, 4, 8, 16 mg/mL EPS for 2 h in a 6-well plate, and then irradiated with the UVB lamp of 250 μw/$cm^2$ for 1 min. After cells were cultured for an additional 24 h, pellet and CFS were collected separately. The relative levels of intracellular ROS were detected by ROS assay kit (YEASEN, Shanghai, China). ELISA kits were used to detect the concentration of IL-1α, IL-1β, IL-6 and IL-8 in the CFS, referring to the operating instructions. HaCaT cells cultured in a 6-well plate were not treated with UVB and EPS as control.

#### 2.6.5. Western blot analysis

The HaCaT cells were treated as described in section 2.6.4 for Western blot analysis. After removing CFS, 400 μL trypsin was added to each well and incubated in the carbon dioxide incubator for 5 min. Then 1 mL medium was added to terminate the reaction and centrifuged to obtain cells at 500 × g for 5 min at 4 °C, the cells were washed twice with cold PBS. After that, the expression levels of phospho-JNK, phospho-p38 MAPKs and active-caspase3 were detected, and GAPDH as the internal standard. HaCaT cells were lysed with RIPA lysate and centrifuged at 12000 × g for 15 min at 4 °C to obtain the crude protein solution. Protein concentrations were tested by BCA kit (Thermo Fisher Scientific, USA) and each sample was adjusted to the same protein concentration. Each sample was loaded with 20 μL into 10% SDS-PAGE for separation and transferred to the PVDF membrane. Subsequently, the PVDF was enclosed with 5% fat-free milk for 1 h, then incubated with primary antibody for 2 h, and finally incubated with secondary antibody (goat anti-rabbit, HRP, ABclonal, China) for 1 h at 37 °C. After the membrane was treated with ECL solution, it was put into a dark box to press the gel, and then the protein band was obtained by scanning with a scanner (K836, BenQ, China).

### 2.7. Statistical analysis

The data are expressed as mean ± standard deviation. The mean value was obtained by one-way analysis of variance (ANOVA) and Duncan's test was performed using SPSS 20.0 software (IBM, Armonk, USA). $P < 0.05$ was considered statistically significant. All experiments were performed in triplicates.

## 3. Result

### 3.1. Screening and identification of LAB producing EPS

We isolated 34 strains of LAB from saliva, as shown in Table 1. A total of 8 strains have the ropy phenotype. Among them, Strain O17 had the highest EPS yield, reaching 0.603 mg/mL. Strain O17 was further characterized as shown in Figure 1. The colony of strain O17 was bulged and smooth (Figure 1A), the bacteria were rod-shaped and Gram-positive (Figure 1B). MALDI TOF MS results showed that the strain O17 had obvious peaks at *m/z* 2946.082, 3476.573, 3791.097, 4692.724, 5892.635, 6953.051, 7581.626, and 9382.474, *etc* (Figure 1C). Autof Acquirer software was used to analyze and compare the results. It was found that the protein expression of strain O17 was the most similar to

**Table 1.** Screening and yield of LAB Producing EPS.

| Strain number | Classification | Ropiness[a] | Yield (mg/mL) | Strain number | Classification | Ropiness[a] | Yield (mg/mL) |
|---|---|---|---|---|---|---|---|
| E01 | *L. plantarum* | - | | O06 | *L. plantarum* | - | |
| E11 | *L. rhamnosus* | - | | O09 | *L. salivarius* | - | |
| E15 | *L. plantarum* | - | | O17 | *L. rhamnosus* | + | 0.603 ± 0.11 |
| E20 | *L. paracasei* | - | | O41 | *L. paracasei* | - | |
| E31 | *L. paracasei* | + | 0.325 ± 0.09 | O42 | *L. fermentum* | - | |
| F03 | *L. casei* | - | | O43 | *L. rhamnosus* | + | 0.397 ± 0.12 |
| F05 | *L. plantarum* | - | | O44 | *L. paracasei* | - | |
| F06 | *L. acidophilus* | - | | O45 | *L. fermentum* | + | 0.314 ± 0.06 |
| F08 | *L. acidophilus* | - | | O46 | *L. fermentum* | - | |
| F10 | *L. plantarum* | - | | O47 | *L. salivarius* | - | |
| F12 | *L. fermentum* | - | | O48 | *L. fermentum* | + | 0.135 ± 0.03 |
| F15 | *L. lactis* | - | | Y06 | *L. rhamnosus* | - | |
| F22 | *L. casei* | - | | Y15 | *L. paracasei* | - | |
| F32 | *L. lactis* | - | | Y20 | *L. rhamnosus* | + | 0.113 ± 0.04 |
| F50 | *L. plantarum* | + | 0.274 ± 0.05 | Y21 | *L. acidophilus* | - | |
| O04 | *L. plantarum* | - | | Y30 | *L. helveticus* | - | |
| O05 | *L. salivarius* | - | | YB32 | *L. brevis* | + | 0.286 ± 0.09 |

[a] +, ropiness phenotype; -, not ropiness phenotype.

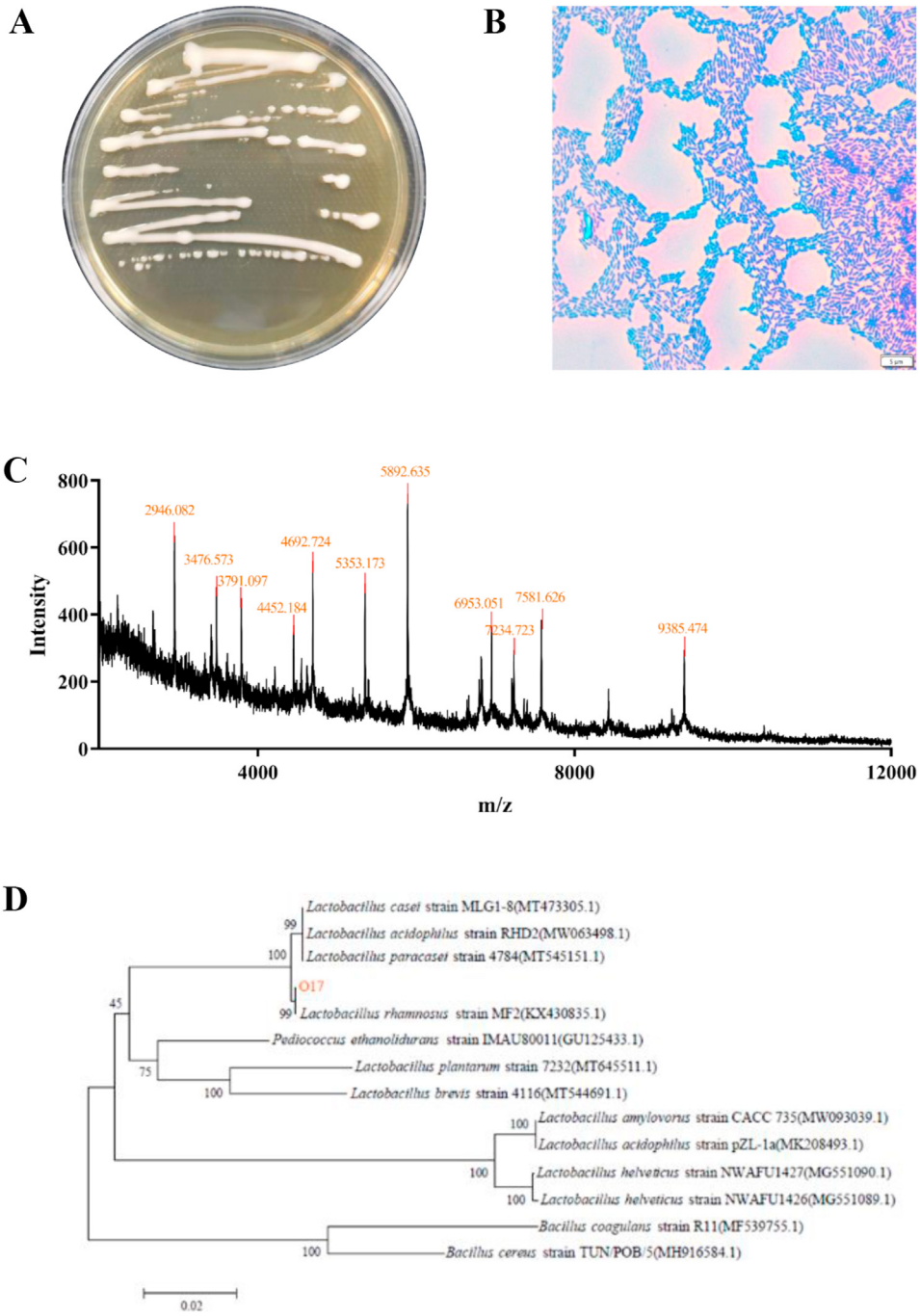


**Figure 1.** Identification of the *Lacticaseibacillus rhamnosus* VHPriobi O17. A, Colonial morphology of *L. rhamnosus* VHPriobi O17. B, Gram staining of *L. rhamnosus* VHPriobi O17. C, Mass spectrum of *L. rhamnosus* VHPriobi O17 by MALDI-TOF MS. D, Phylogenetic tree of *L. rhamnosus* VHPriobi O17 according to the 16S rDNA sequence.

that of *L. rhamnosus*, and the score was 9.536 (scores between 9 and 10 were considered to be effective). The similarity analysis of the 16S rRNA gene showed that the similarity between strain O17 and *L. rhamnosus* MF2 was 99%, and the phylogenetic tree was shown in Figure 1D. The 16S rDNA sequence of strain O17 was submitted to NCBI with the sequence number MZ144127. In summary, strain O17 was identified as *L. rhamnosus* and named as *L. rhamnosus* VHPriobi O17.

### 3.2. Strain growth curve, production and purification of EPS

The growth curve of strain O17 was shown in Figure 2A. The $OD_{600}$ increased slowly from 0 to 8 h, $OD_{600}$ began to increase sharply at 8 h, and $OD_{600}$ no longer increased significantly from 32 to 56 h. In contrast, the concentration of EPS was 0 mg/mL from 0 to 8 h; the concentration of EPS increased rapidly after 8 h and reached the maximum value at 40 h (Figure 2A). Therefore, the CFS of strain O17 cultured for 40 h was used for the purification of EPS.

The CFS of strain O17 was precipitated with alcohol three times and deproteinized with trichloroacetic acid to obtain crude EPS. The crude EPS was further eluted through a DEAE-μSphere chromatography column and the elution curve was shown in Figure 2B. Two kinds of EPS were isolated by chromatographic column, OP-1 was eluted by 0 M NaCl and OP-2 was eluted by 0.05 M NaCl. Through the preliminary experiment, it was found that the anti-UVB activity of OP-1 was much lower than that of

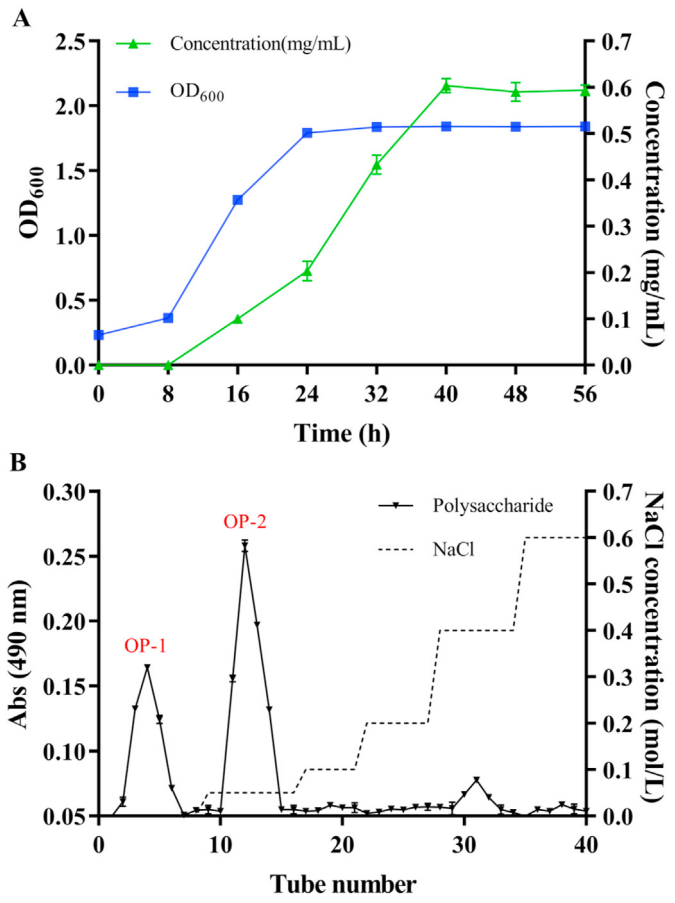


**Figure 2.** A, growth curve and exopolysaccharides (EPS) production of *L. rhamnosus* VHPriobi O17. B, chromatographic diagram of EPS separated by DEAE-μSphere anion exchange Column. Data are presented as the mean ± standard deviation (n = 3).

**Table 2.** The monosaccharide compositions of EPS (OP-2).

| Sugar components | Mole percentage (%) |
|---|---|
| Fuc | nd |
| D-GalN | 2.29 |
| Rha | nd |
| Ara | 1.15 |
| GluN | 3.94 |
| Gal | 2.25 |
| Glc | 7.85 |
| Xyl | nd |
| Man | 82.89 |
| Fru | nd |
| Rib | nd |

OP-2; the content of OP-2 was higher and the degree of separation was higher. Hence, EPS (OP-2) was used in subsequent experiments.

### 3.3. Characterization of EPS

#### 3.3.1. Monosaccharide composition of EPS (OP-2)

The monosaccharide composition of EPS (OP-2) was tested by the ICS5000 ion chromatography system, and the results were shown in Table 2. As shown in Figure 3A, compared with the ion chromatogram of standard monosaccharides, only D-GalN, Ara, GluN, Gal, Glc, and Man were detected in EPS (OP-2) with their molar ratio were 2.29%, 1.15%, 3.94%, 2.25%, 7.85% and 82.89%, respectively (Table 2).

#### 3.3.2. FT-IR analysis of EPS (OP-2)

The FT-IR spectra was shown in Figure 3B. EPS (OP-2) showed a strong and wide absorption peak at 3396.51 $cm^{-1}$, indicating that there was an O—H bond stretching vibration between or within the molecules. The spike near 2933.88 $cm^{-1}$ was caused by C—H stretching vibration. The absorption peaks at 1652.68 $cm^{-1}$ and 1541.63 $cm^{-1}$ were caused by C—O stretching vibration and asymmetric stretching vibration, respectively. The band of 1412.76 $cm^{-1}$, 1382.77 $cm^{-1}$ and 1246.37 $cm^{-1}$ were due to C—H variable-angle vibrations. The band of 1132.11 $cm^{-1}$ indicated the existence of C—O—C stretching vibration in pyranose. The strong absorption peak at 1057.75 $cm^{-1}$ was caused by the bending vibration of the C—O bond in the C—O—H or C—O—C structure, which also proved the existence of pyranoside. The peak at 974.89 $cm^{-1}$ was due to the rolling vibration of the deoxysugar methine, indicating the presence of deoxysugar in EPS (OP-2). The peak at 903.98 $cm^{-1}$ was caused by the C—H angular vibration of the β-terminal isomerization of pyranose. The absorption peak of 812 $cm^{-1}$ is the characteristic peak of β-pyranose with Man residues.

#### 3.3.3. The weight-averaged molecular of EPS (OP-2)

The $M_w$ of EPS (OP-2) was analyzed by gel chromatography. The elution curve was shown in Figure 3C, and a single peak appeared at about 46.8 min. According to the standard curve of Dextran (Figure 3D), the $M_w$ of EPS (OP-2) was calculated to be 84.2 kDa.

### 3.4. The effect of EPS (OP-2) on HaCaT cells

#### 3.4.1. The influence of EPS (OP-2) on cell viability

The toxicity of EPS (OP-2) to HaCaT cells was shown in Figure 4A. The results showed that EPS (OP-2) had no significant effect ($p > 0.05$) on HaCaT cell viability. The viability of HaCaT cells decreased significantly ($p < 0.05$) by UVB radiation in a dose-dependent manner, as shown in Figure 4B, C and D. After treatment with 7.5, 15 and 30 mJ/$cm^2$ UVB, the cell viability decreased to 49.97%, 27.17% and 19.35%, respectively. However, HaCat cells were pre-treated with EPS (OP-2) for 2 h before UVB radiation, and the damage of UVB on cells could be inhibited. For each UVB treatment group, the residual viability of cells increased with the increase in the dose of EPS (OP-2). Moreover, the morphological characteristics of HaCaT cells showed that the number of cells gradually increased with the increase of EPS (OP-2) dose (not shown), which was consistent with the results of the cell viability experiment.

#### 3.4.2. The effect of EPS (OP-2) on intracellular ROS and pro-inflammatory cytokines production

As shown in Figure 5A, UVB exposure rapidly increased intracellular ROS, whereas EPS (OP-2) dose-dependently decreased intracellular ROS in the concentration range of 1–16 mg/mL. The contents of IL-1α, IL-1β, IL-6 and IL-8 in the CFS of the control were relatively low (Figure 5B, C, D and E). After UVB induction, the contents of IL-1α, IL-6 and IL-8 elevated markedly ($p < 0.05$); while IL-1β did not change significantly ($p > 0.05$). With the increase of EPS (OP-2) pretreatment dose, the secretion of three cytokines induced by UVB decreased gradually ($p < 0.05$). The above results showed that EPS (OP-2) pretreatment before UVB irradiation could significantly inhibit intracellular ROS levels and pro-inflammatory cytokines production.

#### 3.4.3. Western blot

In this study, the expression of JNK, p38 MAPK and their downstream apoptotic protein caspase3 in HaCaT cells were assayed, as shown in Figure 6A, B. The results showed that the expression of phospho-JNK, phospho-p38 MAPK and active-caspase3 in HaCaT cells were significantly increased after UVB treatment ($p < 0.05$). But after EPS (OP-2) pretreatment, their expression was inhibited and the inhibitory effect enhanced with the increase of dose.

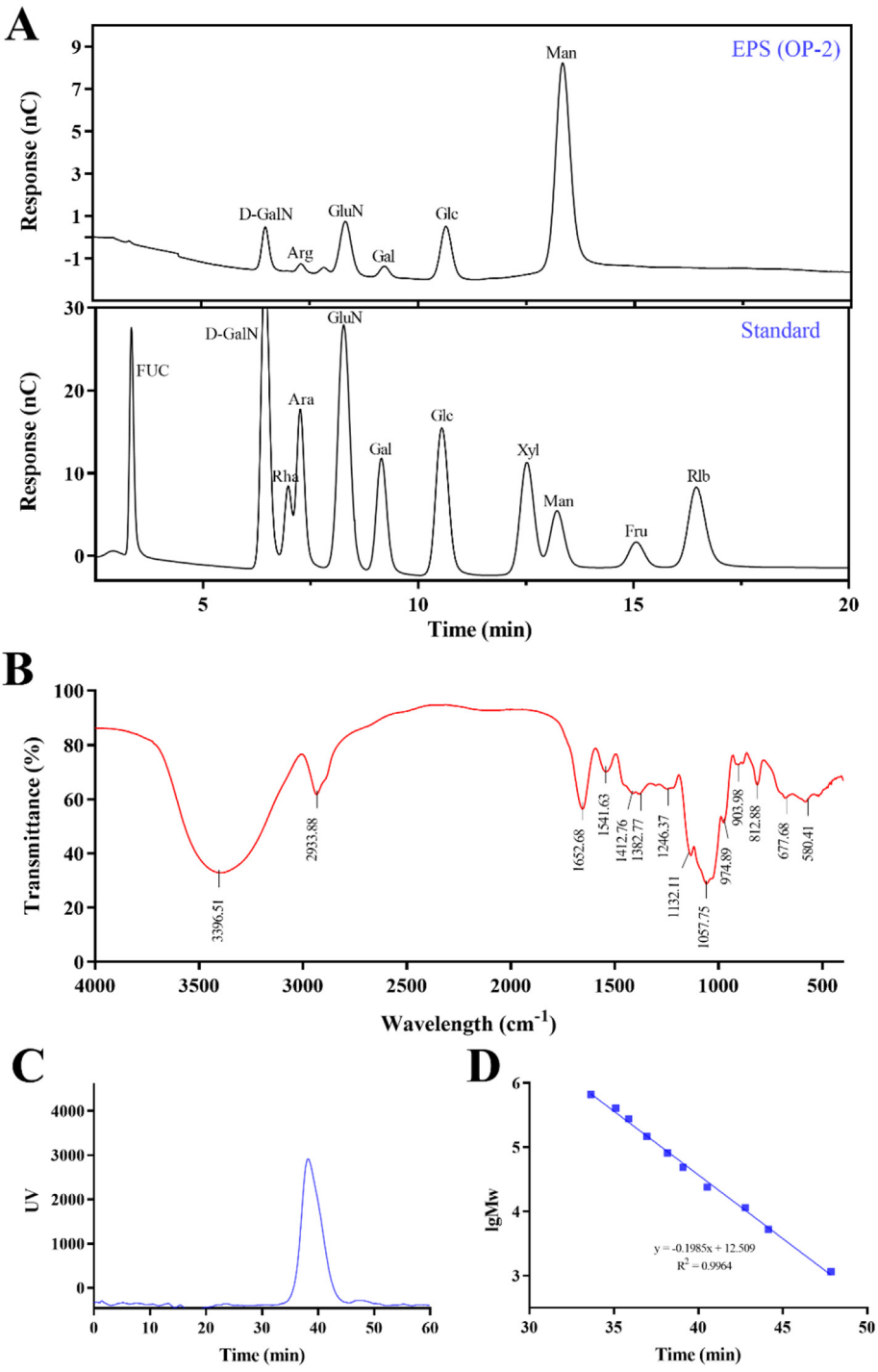


**Figure 3.** Structure characterization of EPS (OP-2) produced by *L. rhamnosus* VHPriobi O17. A, monosaccharide composition. B, FT-IR spectra. C, Gel column chromatogram. D, a standard curve of average molecular weight of the GPC method.

## 4. Discussion

The EPS produced by LAB have been extensively studied due to its good biological activities, such as antioxidant, antitumor and antibacterial [21]. And EPS can also improve the physical and chemical properties of fermented food [22]. In this paper, we screened an *L. rhamnosus* VHPriobi O17 with high-yield EPS. It had been reported that some *L. rhamnosus* can improve human immunity and regulate intestinal flora, such as *L. rhamnosus* GG [23] and *L. rhamnosus* HN001 [24]. In addition, it had also been reported that EPS produced by *L. rhamnosus* LOCK 0900 can inhibit allergic reactions [25]. In this study, we screened strain O17 with EPS production from 34 strains of LAB. The EPS of strain O17 began to produce in the logarithmic phase and reached the maximum in the early stable period, which indicated that the EPS was a secondary metabolite [26]. In addition, the EPS concentration of strain O17 in the CFS was 0.603 mg/mL at 40 h. The EPS yield of this strain was higher than that of *L. rhamnosus* R (0.495 mg/mL) and *L. rhamnosus* C83 (0.1 mg/mL) [27, 28].

Then we purified the EPS (OP-2) and characterized its structure. Previous studies have shown that EPS of LAB were mainly composed of monosaccharides, such as Glu, Man, Gal, Rib and Rha [29]. Our results showed that the EPS (OP-2) produced by strain O17 was a

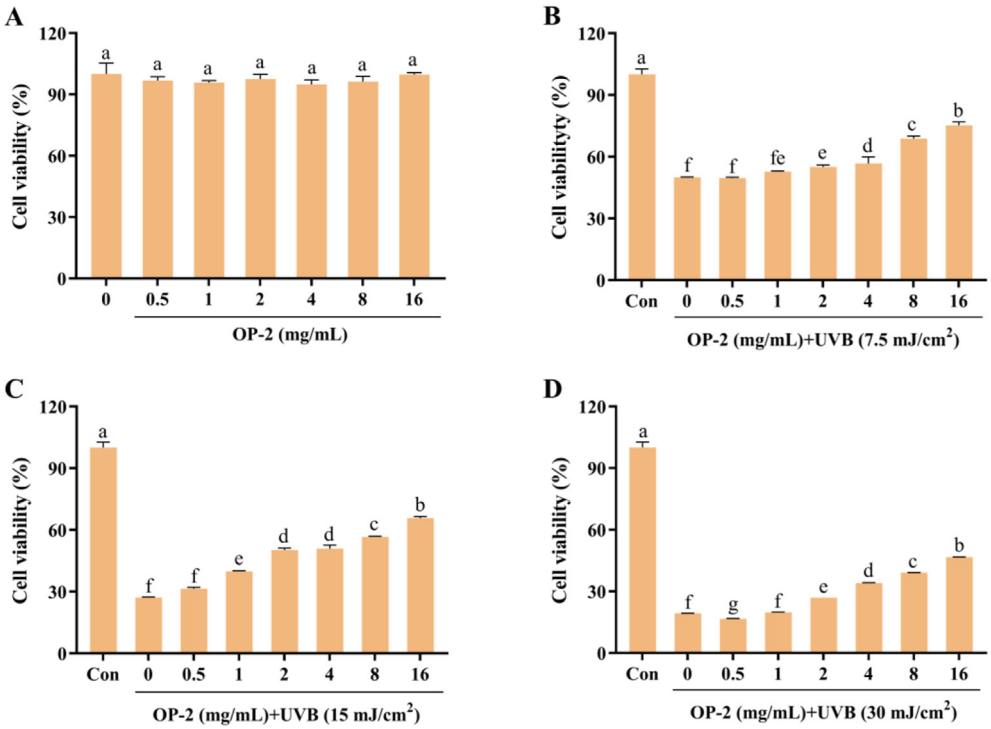


**Figure 4.** A, Toxicity of EPS (OP-2) purified from *L. rhamnosus* VHPriobi O17 to HaCaT cells. B-D, protective effects of EPS (OP-2) on HaCaT cells exposed to UVB (radiation doses are 7.5 mJ/cm$^2$, 15 mJ/cm$^2$, and 30 mJ/cm$^2$, respectively). Data are presented as the mean ± standard deviation (n = 3). Mean values with different letters are significantly different ($p < 0.05$).

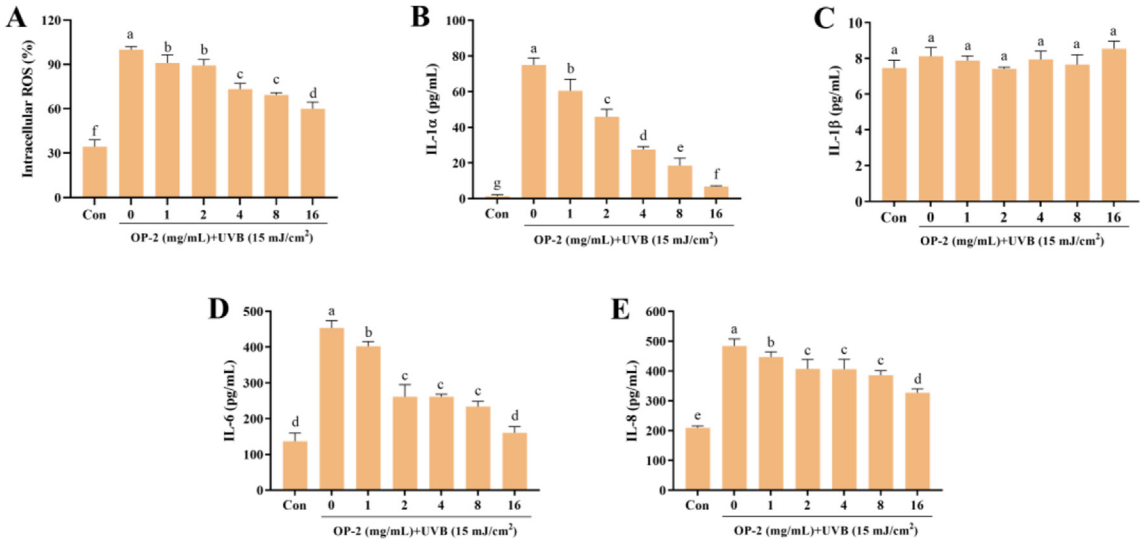


**Figure 5.** Effects of purified EPS (OP-2) from *L. rhamnosus* VHPriobi O17 on intracellular ROS (A), IL-1α (B), IL-1β (C), IL-6 (D), and IL-8 (E) in HaCaT cells exposed to UVB at 15 mJ/cm$^2$. Data are presented as the mean ± standard deviation (n = 3). Mean values with different letters are significantly different ($p < 0.05$).

heteropolysaccharide composed of D-GalN, Ara, GluN, Gal, Glc and Man in a molar ratio of 5:3:9:5:19:198. This is significantly different from the previously reported EPS composition produced by *L. rhamnosus*. For example, the EPS of *L. rhamnosus* JAAS8 is composed of Gal, Glu and N-GluNAc in a ratio of 4:1:1 [30]; *L. rhamnosus* GG is composed of Rha, Gal and 2-deoxysugar-2-amino-D-Glu in a relative ratio of 9:75:16 [31]. Although EPS (OP-2) consisted of six monosaccharides, Man accounted for 82.9%. Therefore, it may be a Man-like polysaccharide. Moreover, it has been reported previously that Man polymers have many health characteristics such as alleviating constipation, absorbing cholesterol, preventing cancer, and enhancing immunity [32]. The functional groups in EPS (OP-2) were quickly and simply identified by FT-IR analysis. From the spectrum, we can see that the spectrum is a typical absorption peak of EPS of LAB. In our study, the FT-IR spectrum of EPS (OP-2) showed strong peaks at 1132.11 and 1057.75 cm$^{-1}$, which were characteristic peaks of Man and positively correlated with the content [33]. This also indicated that EPS (OP-2) contained a large amount of Man, which was consistent with the experimental results of monosaccharide composition. Based on the existing results, we can infer that EPS (OP-2) is mainly composed of β-Man*p*. As far as we know, the EPS secreted by LAB has not been reported with a similar structure. There was a single peak in the elution of the EPS (OP-2) in the gel column, indicating that EPS (OP-2) was

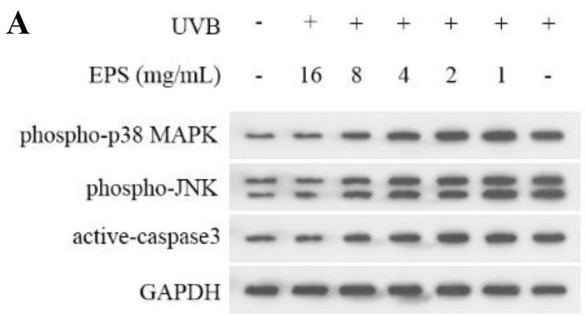


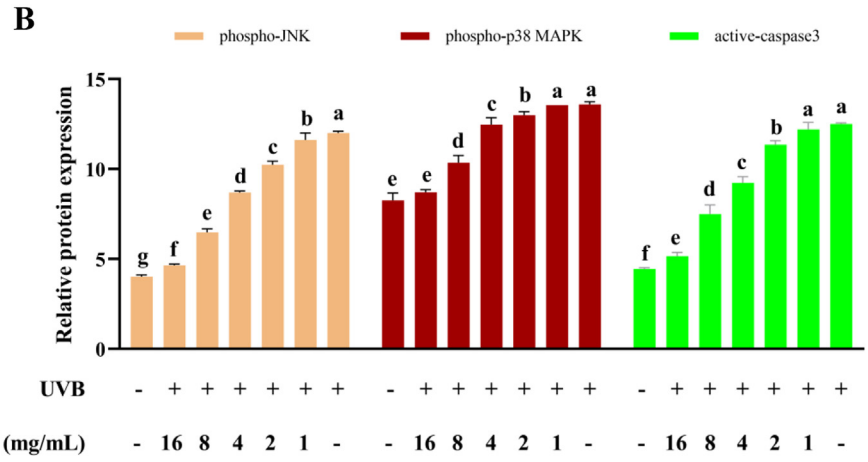


**Figure 6.** Effects of purified EPS (OP-2) from *L. rhamnosus* VHPriobi O17 on the expression in HaCaT cells exposed to UVB at 15 mJ/cm$^2$. A, Representative Western blot for phospho-JNK, phospho-p38 MAPK, and active-caspase3 in cells. B, Quantification of phospho-JNK, phospho-p38 MAPK, and active-caspase3 blots. Data are presented as the mean ± standard deviation (n = 3). Significant differences ($p < 0.05$) are indicated by different letters. The uncropped images of (A) were referred to in supplementary F 1.

relatively pure and homogeneous. The $M_w$ of polysaccharides will affect its biological activity. For example, the antioxidant activity of polysaccharides with low $M_w$ is higher than that with high $M_w$ [34]. The $M_w$ of EPS (OP-2) produced by strain O17 was lower than the reported EPS produced by *L. acidophilus* (152.64 kDa), *L. casei* (178.72 kDa), *L. mesenteroides* (123.84 kDa) and *L. lactis* (131.44 kDa) [14]; far lower than *L. plantarum* AR307 (605 kDa) [35]. In conclusion, EPS (OP-2) produced by strain VHPriobi O17 should be a novel Man-like polysaccharide with health effects.

It is well known that UVB irradiation can induce skin damage. If people do not pay attention to protection, it can cause a variety of skin diseases, which can eventually lead to skin cancer. In this study, we demonstrated that EPS (OP-2) from strain VHPriobi O17 inhibited UVB-induced skin cell death and explored the potential mechanism. Our results suggested that UVB irradiation could remarkably reduce the viability of HaCaT cells, the residual viability decreased with the increase of UVB dose, and similar results can be seen in previous studies [36]. Oxidative stress induced by UVB radiation results in excessive production of intracellular ROS in skin cells, causing cells damage and eventually apoptosis [37]. Our results also showed that intracellular ROS increased rapidly after exposure to UVB. Our previous study found that EPS (OP-2) not only had obvious scavenging activity on DPPH and hydroxyl radical, but also inhibited lipid peroxidation (data not shown). So we further explored the effect of EPS on UVB-induced intracellular ROS. The results showed that EPS (OP-2) effectively suppressed UVB-induced elevation of intracellular ROS. Therefore, EPS reduced intracellular ROS due to its antioxidant activity, thereby alleviating the damage of UVB on skin cells.

Intracellular ROS generated by UVB irradiation regulates a variety of protein phosphorylation signaling pathways [38]. Simon et al. found that ROS indirectly or directly mediated caspase activation [39]. In addition, Okayama believed that intracellular ROS also plays an important role in skin inflammatory response [40]. Therefore, ROS should be an important medium for UVB-induced inflammatory response and apoptosis. In this research, we observed that HaCaT cells increased the production of IL-1α, IL-6 and IL-8 after exposure to UVB. However, there was no significant change in the production of IL-1β, inconsistent with the results reported by Kim et al. [41], which may be due to the difference in individuals from cell sources. Moreover, the production of IL-1α, IL-6 and IL-8 was inhibited after pretreatment with EPS (OP-2). This suggested that EPS (OP-2) reduced intracellular ROS level, furthermore inhibited IL-1α, IL-6 and IL-8 secretion to relieve UVB-induced HaCaT cells injury.

Apoptosis is a regulated process that allows cells to self-degrade so that the body can eliminate unwanted or dysfunctional cells, and its internal pathway is initiated by intracellular mitochondrial release signal factors [42]. Previous reports have confirmed that UVB can activate MAPK signaling pathway to induce apoptosis [43]. Among them, JNK and p38 MAPK are mainly involved in cell responses to inflammation or stress signals, including pro-inflammatory cytokines and UV irradiation [44]. Caspase3 is a member of the caspase family that promotes irreversible apoptosis after activation [45]. Li et al. found that liquiritin inhibits UVB-induced skin injury by inhibiting the MAPK/caspase3 signaling pathway to inhibit apoptosis [46]. More and more evidence also shows that ROS induced by UVB radiation acts as the second messenger of MAPK signaling pathway activation [47]. Our data suggested that EPS (OP-2) may protect cells from UVB-induced apoptosis by reducing intracellular ROS, thereby inhibiting the expression of phospho-JNK and phospho-p38 MAPK and weakening active-caspase3. It should be noted that EPS from *Pantoea agglomerans* also has similar anti-UVB effects, but only activates JNK rather than p38 MAPK [6]. In addition, some studies believed that the production of pro-inflammatory cytokines was also mediated by the MAPK signaling pathway. A previous study found that the p38 MAPK pathway mediated IL-6, IL-8 and Cox-2 production [48]. However, Kim et al. reported that UVB induced a significant increase in IL-6 after treatment with a p38 MAPK inhibitor [49]. Although the expression of phospho-p38 MAPK and secretion of IL-6 and IL-8 were significantly decreased after pretreatment with EPS (OP-2) in

this study, whether pro-inflammatory cytokines were mediated by MAPK signaling pathway needs further verification. Furthermore, the clinical efficacy of EPS (OP-2) in the body also needs to be further explored.

## 5. Conclusion

We screened an *L. rhamnosus* with high-yield EPS and named it *L. rhamnosus* VHPriobi O17. The EPS (OP-2) was a novel Man-like polysaccharide with a weight-averaged molecular of 84.2 kDa. It can inhibit the generation of intracellular ROS in UVB-irradiated HaCaT cells; reduce the production of IL-1α, IL-6 and IL-8 to reduce inflammatory response; meanwhile, arrest the activation of caspase3 through JNK and p38 MAPK signaling pathways, which ultimately prevented apoptosis. Our results showed that *L. rhamnosus* VHPriobi O17 and its EPS have significant health benefits on human skin.

## Declarations

### *Author contribution statement*

Shudong Peng: Conceived and designed the experiments; Performed the experiments; Analyzed and interpreted the data; Contributed reagents, materials, analysis tools or data; Wrote the paper.

Chaoqun Guo: Analyzed and interpreted the data; Contributed reagents, materials, analysis tools or data.

Songjie Wu: Contributed reagents, materials, analysis, tools or data.

Zhi Duan: Conceived and designed the experiments; analysis tools or data; Wrote the paper.

### *Funding statement*

This work was supported by the Mountain Tai New Strategy Industry Leader Program (Grant No. tscy20180317).

### *Data availability statement*

Data included in article/supp. material/referenced in article.

### *Declaration of interest's statement*

The authors declare no conflict of interest.

### *Additional information*

Supplementary content related to this article has been published online at https://doi.org/10.1016/j.heliyon.2022.e11125.

## Acknowledgements

We wish to acknowledge Dr. Ying Chen (School of Food Science and Engineering, South China University of Technology) for his helpful comments on this manuscript.

## References

[1] L. Verschooten, S. Claerhout, A. Van Laethemii, P. Agostinis, M. Garmyn, Invited review new strategies of photoprotection, Photochem. Photobiol. 82 (2006) 1016–1023.

[2] S. Salucci, S. Burattini, M. Battistelli, V. Baldassarri, M.C. Maltarello, E. Falcieri, Ultraviolet B (UVB) irradiation-induced apoptosis in various cell lineages in vitro, Int. J. Mol. Sci. 14 (2013) 532–546.

[3] A. Kammeyer, R.M. Luiten, Oxidation events and skin aging, Ageing Res. Rev. 21 (2015) 16–29.

[4] W. Liu, F. Wang, C. Li, W. Otkur, T. Hayashi, K. Mizuno, S. Hattori, H. Fujisaki, S. Onodera, T. Ikejima, Silibinin treatment protects human skin cells from UVB injury through upregulation of estrogen receptors, J. Photochem. Photobiol. B Biol. 216 (2021), 112147.

[5] Z. Xiao, S. Yang, J. Chen, C. Li, C. Zhou, P. Hong, S. Sun, Z.J. Qian, Trehalose against UVB-induced skin photoaging by suppressing MMP expression and enhancing procollagen I synthesis in HaCaT cells, J. Funct.Foods 74 (2020), 104198.

[6] L. Li, T. Huang, H. Liu, J. Zang, P. Wang, X. Jiang, Purification, structural characterization and anti-UVB irradiation activity of an extracellular polysaccharide from *Pantoea agglomerans*, Int. J. Biol. Macromol. 137 (2019) 1002–1012.

[7] Y.M. Kang, C.H. Hong, S.H. Kang, D.S. Seo, S.O. Kim, H.Y. Lee, H.J. Sim, H.J. An, Anti-photoaging effect of plant extract fermented with *Lactobacillus buchneri* on CCD-986sk fibroblasts and HaCaT keratinocytes, J. Funct. Biomater. 11 (2020) 1–12.

[8] C. Hill, F. Guarner, G. Reid, G.R. Gibson, D.J. Merenstein, B. Pot, L. Morelli, R.B. Canani, H.J. Flint, S. Salminen, P.C. Calder, M.E. Sanders, Expert consensus document: the international scientific association for probiotics and prebiotics consensus statement on the scope and appropriate use of the term probiotic, Nat. Rev. Gastroenterol. Hepatol. 11 (2014) 506–514.

[9] G.H. Van Geel-Schutten, F. Flesch, B. Ten Brink, M.R. Smith, L. Dijkhuizen, Screening and characterization of *Lactobacillus* strains producing large amounts of exopolysaccharides, Appl. Microbiol. Biotechnol. 50 (1998) 697–703.

[10] X. Wang, C. Shao, L. Liu, X. Guo, Y. Xu, X. Lü, Optimization, partial characterization and antioxidant activity of an exopolysaccharide from *Lactobacillus plantarum* KX041, Int. J. Biol. Macromol. 103 (2017) 1173–1184.

[11] H. Ispirli, E. Dertli, Detection of fructophilic lactic acid bacteria (FLAB) in bee bread and bee pollen samples and determination of their functional roles, J. Food Process. Preserv. 45 (2021) 1–11.

[12] W. Di, L. Zhang, H. Yi, X. Han, Y. Zhang, L. Xin, Exopolysaccharides produced by *Lactobacillus* strains suppress HT-29 cell growth via induction of G0/G1 cell cycle arrest and apoptosis, Oncol. Lett. 16 (2018) 3577–3586.

[13] M. Dinic, U. Pecikoza, J. Djokic, R. Stepanovic-Petrovic, M. Milenkovic, M. Stevanovic, N. Filipovic, J. Begovic, N. Golic, J. Lukic, Exopolysaccharide produced by probiotic strain *Lactobacillus paraplantarum* BGCG11 reduces inflammatory hyperalgesia in rats, Front. Pharmacol. 9 (2018) 1–12.

[14] X. Yang, Y. Ren, L. Zhang, Z. Wang, L. Li, Structural characteristics and antioxidant properties of exopolysaccharides isolated from soybean protein gel induced by lactic acid bacteria, LWT (Lebensm.-Wiss. & Technol.) 150 (2021), 111811.

[15] S. Ramamoorthy, A. Gnanakan, S.S. Lakshmana, M. Meivelu, A. Jeganathan, Structural characterization and anticancer activity of extracellular polysaccharides from ascidian symbiotic bacterium *Bacillus thuringiensis*, Carbohydr. Polym. 190 (2018) 113–120.

[16] J. Song, S. Peng, J. Yang, F. Zhou, H. Suo, Isolation and identification of novel antibacterial peptides produced by *Lactobacillus fermentum* SHY10 in Chinese pickles, Food Chem. 348 (2021), 129097.

[17] S. Peng, J. Song, W. Zeng, H. Wang, Y. Zhang, J. Xin, H. Suo, A broad-spectrum novel bacteriocin produced by *Lactobacillus plantarum* SHY 21–2 from yak yogurt: purification, antimicrobial characteristics and antibacterial mechanism, LWT 142 (2021), 110955.

[18] M. Ayyash, B. Abu-Jdayil, A. Olaimat, G. Esposito, P. Itsaranuwat, T. Osaili, R. Obaid, J. Kizhakkayil, S.Q. Liu, Physicochemical, bioactive and rheological properties of an exopolysaccharide produced by a probiotic *Pediococcus pentosaceus* M41, Carbohydr. Polym. 229 (2020), 115462.

[19] M.S. Riaz Rajoka, H.M. Mehwish, H. Fang, A.A. Padhiar, X. Zeng, M. Khurshid, Z. He, L. Zhao, Characterization and anti-tumor activity of exopolysaccharide produced by *Lactobacillus kefiri* isolated from Chinese kefir grains, J. Funct.Foods 63 (2019), 103588.

[20] I. Mitra, S. Mukherjee, P.B. Reddy Venkata, S. Dasgupta, C.K. Jagadeesh Bose, S. Mukherjee, W. Linert, S.C. Moi, Benzimidazole based Pt (II) complexes with better normal cell viability than cisplatin: synthesis, substitution behavior, cytotoxicity, DNA binding and DFT study, RSC Adv. 6 (2016) 76600–76613.

[21] K. Abdhul, M. Ganesh, S. Shanmughapriya, M. Kanagavel, K. Anbarasu, K. Natarajaseenivasan, Antioxidant activity of exopolysaccharide from probiotic strain *Enterococcus faecium* (BDU7) from Ngari, Int. J. Biol. Macromol. 70 (2014) 450–454.

[22] H. İspirli, O. Sagdic, M.T. Yılmaz, E. Dertli, Physicochemical characterisation of an α-glucan from *Lactobacillus reuteri* E81 as a potential exopolysaccharide suitable for food applications, Process Biochem 79 (2019) 91–96.

[23] V.M. Castro-Herrera, H.L. Fisk, M. Wootton, M. Lown, E. Owen-Jones, M. Lau, R. Lowe, K. Hood, D. Gillespie, F.D.R. Hobbs, P. Little, C.C. Butler, E.A. Miles, P.C. Calder, Combination of the probiotics *Lacticaseibacillus rhamnosus* GG and *Bifidobacterium animalis* subsp. *lactis*, BB-12 has limited effect on biomarkers of immunity and inflammation in older people resident in care homes: results from the probiotics to reduce inf, Front. Immunol. 12 (2021) 1–10.

[24] M.L. Cross, R.R. Mortensen, J. Kudsk, H.S. Gill, Dietary intake of *Lactobacillus rhamnosus* HN001 enhances production of both Th1 and Th2 cytokines in antigen-primed mice, Med. Microbiol. Immunol. 191 (2002) 49–53.

[25] S. Górska, M. Schwarzer, D. Srutkova, P. Hermanova, E. Brzozowska, H. Kozakova, A. Gamian, Polysaccharides L900/2 and L900/3 isolated from *Lactobacillus rhamnosus* LOCK 0900 modulate allergic sensitization to ovalbumin in a mouse model, Microb. Biotechnol. 10 (2017) 586–593.

[26] L. Yi, J. Dang, L. Zhang, Y. Wu, B. Liu, X. Lü, Purification, characterization and bactericidal mechanism of a broad spectrum bacteriocin with antimicrobial activity against multidrug-resistant strains produced by *Lactobacillus coryniformis* XN8, Food Control 67 (2016) 53–62.

[27] P.L. Pham, I. Dupont, D. Roy, G. Lapointe, J. Cerning, Production of exopolysaccharide by *Lactobacillus rhamnosus* R and analysis of its enzymatic degradation during prolonged fermentation, Appl. Environ. Microbiol. 66 (2000) 2302–2310.

[28] L. Gamar, K. Blondeau, J.M. Simonet, Physiological approach to extracellular polysaccharide production by *Lactobacillus rhamnosus* strain C83, J. Appl. Microbiol. 83 (1997) 281–287.

[29] Y. Tang, W. Dong, K. Wan, L. Zhang, C. Li, L. Zhang, N. Liu, Exopolysaccharide produced by *Lactobacillus plantarum* induces maturation of dendritic cells in BALB/c mice, PLoS One 10 (2015) 1–16.
[30] Z. Yang, S. Li, X. Zhang, X. Zeng, D. Li, Y. Zhao, J. Zhang, Capsular and slime-polysaccharide production by *Lactobacillus rhamnosus* JAAS8 isolated from Chinese sauerkraut: potential application in fermented milk products, JBIOSC 110 (2010) 53–57.
[31] C. Landersjö, Z. Yang, E. Huttunen, G. Widmalm, Structural studies of the exopolysaccharide produced by *Lactobacillus rhamnosus* strain GG (ATCC 53103), Biomacromolecules 3 (2002) 880–884.
[32] M. Li, J. Du, Y. Han, J. Li, J. Bao, K. Zhang, Non-starch polysaccharides in commercial beers on China market: mannose polymers content and its correlation with beer physicochemical indices, J. Food Compos. Anal. 79 (2019) 122–127.
[33] M.A. Coimbra, A.S. Barros, E. Coelho, F. Gonçalves, S.M. Rocha, I. Delgadillo, Quantification of polymeric mannose in wine extracts by FT-IR spectroscopy and OSC-PLS1 regression, Carbohydr. Polym. 61 (2005) 434–440.
[34] N.M. El-Deeb, A.M. Yassin, L.A. Al-Madboly, A. El-Hawiet, A novel purified *Lactobacillus acidophilus* 20079 exopolysaccharide, LA-EPS-20079, molecularly regulates both apoptotic and NF-κB inflammatory pathways in human colon cancer, Microb. Cell Factories 17 (2018) 1–15.
[35] X. Feng, H. Zhang, P.F.H. Lai, Z. Xiong, L. Ai, Structure characterization of a pyruvated exopolysaccharide from *Lactobacillus plantarum* AR307, Int. J. Biol. Macromol. 178 (2021) 113–120.
[36] Z. Liu, M. Jiang, J. Zhao, Q. Wang, C. Zhang, M. Gao, M. Gu, L. Xiang, Efficacy of a wound-dressing biomaterial on prevention of postinflammatory hyperpigmentation after suction blister epidermal grafting in stable vitiligo patients: a controlled assessor-blinded clinical study with in vitro bioactivity investigation, Arch. Dermatol. Res. 312 (2020) 635–645.
[37] N. Minamisawa, M. Ming-San, K. Le, L. Hui-Juan, C. Lin-Lin, H. Kanemisu, T. Naito, H. Shinotsuka, Protective effects of jin Bai mei yan prescription on oxidative damage and photoaging induced by ultraviolet B in HaCaT cells, digit, Chin. Med. 3 (2020) 57–66.
[38] Y. Zhai, Y. Dang, W. Gao, Y. Zhang, P. Xu, J. Gu, X. Ye, P38 and JNK Signal Pathways Are Involved in the Regulation of Phlorizin against UVB-Induced Skin Damage, (n.d.).
[39] H. Simon, A. Haj-Yehia, F. Levi-Schaffer, Role of reactive oxygen species (ROS) in apoptosis induction, Apoptosis 5 (2000) 415–418.
[40] Y. Okayama, Oxidative stress in allergic and inflammatory skin diseases, Curr. Drug Targets - Inflamm. Allergy 4 (2005) 517–519.
[41] D. Kim, R. Hu, Y. Fan, Y. Xu, H. Joo, S. Kook, Photoprotective effects of 2S,3R-6-methoxycarbonylgallocatechin isolated from Anhua dark tea on UVB-induced inflammatory responses in human keratinocytes, J. Photochem. Photobiol. B Biol. 202 (2020), 111704.
[42] C. Lin, R.E.H. Jr, J.C. Donofrio, M.H. Mccoy, L.R. Tudor, T.M. Chambers, Caspase activation in equine influenza virus induced apoptotic cell death 84, 2002, pp. 357–365.
[43] D. Decraene, K. Smaers, D. Gan, T. Mammone, M. Matsui, D. Maes, L. Declercq, M. Garmyn, A synthetic superoxide dismutase/catalase mimetic (EUK-134) inhibits membrane-damage-induced activation of mitogen-activated protein kinase pathways and reduces p53 accumulation in ultraviolet B-exposed primary human keratinocytes, J. Invest. Dermatol. 122 (2004) 484–491.
[44] J.M. Kyriakis, J. Avruch, Mammalian mitogen-activated protein kinase signal transduction pathways activated by stress and inflammation, Physiol. Rev. 81 (2001) 807–869.
[45] A.G. Porter, R.U. Jänicke, Emerging roles of caspase-3 in apoptosis, Cell Death Differ. 6 (1999) 99–104.
[46] X.Q. Li, L.I.M.I.N. Cai, J. Liu, Y.A.N.L.I. Ma, Y.H.U.I. Kong, H.E. Li, M. Jiang, Liquiritin Suppresses UVB-Induced Skin Injury through Prevention of Inflammation, Oxidative Stress and Apoptosis through the TLR4/MyD88/NF-Kb and MAPK/caspase Signaling Pathways, 2018, pp. 1445–1459.
[47] L. Li, T. Huang, C. Lan, H. Ding, C. Yan, Y. Dou, Protective effect of polysaccharide from Sophora japonica *L. flower* buds against UVB radiation in a human keratinocyte cell line (HaCaT cells), J. Photochem. Photobiol. B Biol. 191 (2019) 135–142.
[48] L. Jinlian, Z. Yingbin, W. Chunbo, p38 MAPK in regulating cellular responses to ultraviolet radiation, J. Biomed. Sci. 14 (2007) 303–312.
[49] Y. Kim, S. Koo, S. Bae, H. Kim, Y. Park, N. Kyun, S.G. Kim, H. Kim, Y. Hwang, J. Seung, W. Jae, The anti-inflammatory effect of alloferon on UVB-induced skin inflammation through the down-regulation of pro-inflammatory cytokines, Immunol. Lett. 149 (2013) 110–118.